Frontiers in Heat and Mass Transfer

Tech Science Press

DOI: 10.32604/fhmt.2024.057924

ARTICLE

First and Second Law Analysis of a LiBr-Water Absorption Cycle with Recovering Condensation Heat for Generation

J. L. Rodríguez-Muñoz[1,*], J. S. Pacheco-Cedeño[1,*], J. F. Ituna-Yudonago[2], J. J. Ramírez-Minguela[3] and I. J. González-Hernández[4]

[1]Department of Mechanical Engineering, Escuela Superior de Ciudad Sahagún, Universidad Autónoma del Estado de Hidalgo, Ciudad Sahagún, Carretera Cd. Sahagún-Otumba s/n, Zona Industrial, Hidalgo, C.P. 43998, México

[2]Departamento de Ingeniería en Aeronáutica, Universidad Politécnica Metropolitana de Hidalgo, Boulevard Acceso a Tolcayuca 1009, Ex Hacienda de San Javier Tolcayuca, Hidalgo, C.P. 43860, México

[3]Department of Chemical Engineering, University of Guanajuato, DCNE, Col. Noria Alta s/n, Guanajuato, Gto., C.P. 36050, México

[4]Department of Industrial Engineering, Escuela Superior de Ciudad Sahagún, Universidad Autónoma del Estado de Hidalgo, Ciudad Sahagún, Hidalgo, C.P. 43998, México

*Corresponding Authors: J. L. Rodríguez-Muñoz. Email: jose_rodriguez@uaeh.edu.mx; J. S. Pacheco-Cedeño. Email: sergio_pacheco@uaeh.edu.mx

Received: 31 August 2024 Accepted: 12 October 2024 Published: 19 December 2024

ABSTRACT

In conventional absorption refrigeration systems (*ARS*), the heat from the condenser is usually rejected by the environment in place to be used in the system, so recuperating this is a good alternative to enhance the system's performance. For instance, in this paper, an alternative *ARS* in which LiBr/Water is used as a refrigerant mixture, where part of condensing heat is recovered via the solution heat recovery generator absorption cycle (*HR-ARS*) was energy and exergy evaluated. The influence of generator, condenser and evaporator temperatures, as well as the efficiency of the solution heat exchanger on the coefficient of performance, exergy performance and exergy destroyed of the *HR-ARS* system, were analyzed and compared with the traditional ARS system at the same working conditions. The results showed an increase between 5.8%–6.3% on the *COP* and 3.7%–9.5% in the exergy efficiency when condenser/absorber temperature was reduced from 40°C to 30°C. However, when the evaporation temperature rose from 5°C to 15°C, the *COP* (coefficient of performance) increased by around 8%, although this could be increased by 2.3%–6.3% if the generator temperature decreases from 100°C to 80°C. Moreover, the *COP* and exergetic performance for the *HR-ARS* is more significant at the lowest generator, condenser and evaporator temperatures, as well as at high efficiency in the solution heat exchanger, in comparison to *ARS* system. Furthermore, the *COP* and exergy performance for the *HR-ARS* system was improved by 2.57% to 3.11% and 0.22% to 0.7%, respectively, while the recovering condensation heat for generation is around 1.51%–3.76% lower than with the *ARS*. It also was found that for all ranges of evaporator and condenser temperatures, the *COP* for the *HR-ARS* system is around 3% higher than that obtained with the *ARS* at the three different generator temperatures here analyzed, while when the solution heat exchanger effectiveness was increased from 0.7–1.0, the total exergy destruction for the *HR-ARS* resulted be 3.24%–5.01% smaller than the *ARS* system. Finally, it can be concluded that the components with the most exergy destroyed in the systems (80% to 94%) are the generator and absorber.

KEYWORDS
Absorption refrigeration system; recovery condensation heat; energy and exergy analysis; LiBr-H_2O

Nomenclature

COP	Coefficient of performance (–)
e	Specific exergy (kJ kg^{-1})
I	Exergy destruction (kW)
h	Enthalpy (kJ kg^{-1})
$\dot{m}$	Flow mass rate (kg s^{-1})
P	Pressure (bar)
$\dot{Q}$	Heat transfer rate (kW)
s	Specific entropy (kJ kg^{-1} K^{-1})
T	Temperature (°C)
$\dot{W}$	Power (kW)
x	Mass concentration (%)

Greek Symbols

η	Efficiency (%)

Subscripts

0	Reference state
1,2,$\cdots$	Thermodynamic states
e	Exit
i	Inlet
AB	Absorber
C	Condenser
E	Evaporator
F	Fuel
GE	Generator
P	Product
r	Refrigerated object
SP	Solution pump
SEV	Solution expansion valve
SHX	Solution heat exchanger
Total	Total

1 Introduction

The worldwide energy demand in the industrial sector and households has been growing rapidly during the last few years [1,2]. In majority of these society sectors use refrigeration and air conditioning systems based on vapor compression technology to keep their comfort conditions, however, they consume around 30% of the electricity produced [3]. To save electricity, absorption refrigeration

systems are becoming a viable alternative because they can use waste heat from thermal systems or solar energy [4] and they can use refrigerants with low or null global warming potential, which could be considered an ecological refrigeration technology [5,6].

The most common absorption refrigeration technology uses LiBr-Water and NH_3-Water as working fluids, where LiBr-Water mixture is employed for air conditions applications [7], while NH_3-Water mixture is commonly used for refrigeration applications [8]. Nevertheless, LiBr/H_2O mixture exhibits higher energy performance than NH_3/H_2O [9,10]. Furthermore, the challenge with the absorption systems is to improve their energy performance so that they can be competitive in comparison with the traditional vapor compression chillers. For this reason, various authors have published works where energy analysis has been applied to absorption refrigeration systems.

Ayou et al. [11] made an energy study in a LiBr-Water reversible absorption refrigeration system for cooling, ventilation and household hot water modes. The proposed configuration is to improve the operation time and the primary energy in a LiBr-Water single effect *ARS* driven by an evacuated solar tube collector. Their results revealed that the generator temperature is a critical factor in the system performance, then, a generator temperature of 110°C is required to obtain the highest *COP* of 0.74 without solution crystallization risk. Ahmad et al. [12] made a detailed energy analysis for a single effect LiBr-Water *ARS* under different climate conditions and the results were compared with the LiCl-Water mixture. The optimum *COP* for the LiBr-Water system ranged between 0.74 to 0.90 and for the LiCl-Water cycle was 0.809 to 0.926 at the minimum generator temperature of 54.56°C and 26.25°C, respectively.

Jeong et al. [13] investigated a hybrid cooling/heating absorption heat pump using LiBr/Water as a refrigerant mixture. The *COP* for the hybrid heat pump was found superior to the conventional single effect *ARS*. Wang et al. [14] evaluated thermodynamically a novel combined cooling and power *ARS*, where an ejector was incorporated at the lower turbine back pressure. This configuration showed an increase of 13% in the electricity produced and 45% in the thermal performance, in comparison with a similar system without an ejector. Razmi et al. [15] analyzed a hybrid absorption/recompression cycle, where the generator and compressor were compacted, avoiding the use of the condenser and improving the *COP* considerably. Furthermore, Babaei et al. [16] presented a thermodynamic simulation to predict the *COP* and exergy efficiency in an innovative absorption-recompression chiller where Fe, Al_2O_3 and SiO_2 nanoparticles were dissolved in LiBr-Water mixture. They concluded that Fe-LiBr-Water mixture can improve 14.6% and 18% of the energy performance and electricity consumption in the compressor when compared with the other two. Peng et al. [17] evaluated a hybrid absorption chiller, employing low grade-heat to reduce the work in the compressor. The proposed novel system resulted in a reduction of 9.3% and 10.45% in the compressor energy consumption in comparison with the two-stage compression chiller and the cascade absorption-compression chiller. To reduce the thermal load in the condenser, Wang et al. [18] incorporated two compressors between the generator and the condenser and this configuration was named absorption-compression refrigeration hybrid cycle (*RCHG-ARS*). They compared the energetic efficiency of the alternative cycle with those of the basic *ARS* under different working conditions. Their results evidenced that the thermal load in the generator can be reduced between 70%–80% and the *COP* enhanced by 97.1%, in comparison with the ARS.

Other studies evaluate the exergetic efficiency and quantify the irreversibilities in absorption refrigeration cycles from the second thermodynamics point of view. In this sense, Pacheco-Cedeño et al. [19] applied an exergetic study to the configuration proposed by Wang et al. [18]. According to their analysis, the *RCHG-ARS* presented 0.20% higher exergetic performance than *ARS* at the lowest

generator pressure (P_{GE} = 5.94 bar), although the lowest relative exergy destroyed was found at high generation and condensing temperatures (100°C and 40°C) and an evaporating temperature of −5°C. Ochoa et al. [20] presented an exergy study in a LiBr-Water single effect ARS by varying the ambient temperature from 10°C to 50°C. Derived from their study, the authors found that the solution heat exchanger presented the highest exergy destroyed and the maximum exergetic efficiency was found in the generator. Blanco-Marigorta et al. [21] studied the key aspects of the exergy analysis for each of the components in different LiBr-Water absorption refrigeration cycles under different ambient temperatures. Their results revealed that the exergy destruction in the system can present some differences according to the methodology applied. Banu et al. [22] developed a detailed exergy analysis approach in a LiBr-Water absorption chiller to evaluate the irreversibilities of each cycle. Likewise, Mohtaram et al. [23] conducted an exergy analysis in an *ARS* using LiBr-Water as working fluid. According to their simulation results, the absorber showed 35.87% of the total exergy destruction in the system, due to the low efficiency of this component, then it is recommended to pay attention to the outlet exergy of this component.

According to the literature, analyzing absorption refrigeration cycles from the first and second laws of thermodynamics is necessary to determine the best energy and exergy performance, as well as the irreversibilities presented in the system. So, this work aims to analyze an alternative *ARS*, where part of the thermal load in the condenser is recovered via the solution heat exchanger and supplied into the generator (*HR-ARS*), in which LiBr/Water is used as a refrigerant mixture. The results obtained are contrasted with those of traditional *ARS* under the same operating conditions. Furthermore, some parameters such as generator, condenser/absorber and evaporator temperatures as well as the efficiency of the solution heat exchanger on the coefficient of performance and exergetic efficiency are examined and compared with the conventional *ARS*.

Finally, those parameters also were investigated on the entropy generation in the system, because these are very important to identify and minimize the thermodynamic losses, which can enhance the performance of the system.

2 Thermodynamic Analysis of the Systems

2.1 Operating Principle

Fig. 1a,b shows the representation of traditional and alternative absorption refrigeration systems. The systems consist of the eight basic components: generator (GE), condenser (CO), evaporator (E), absorber (AB), solution pump (SP), solution throttling valve (SEV), solution heat exchanger (SHX) and refrigerant throttling valve (REV). It is important to point out that the operating principle of the conventional ARS cycle is very similar to the alternative HR-ARS cycle. First, in the evaporator the refrigerant exits as saturated vapor (10) and then enters the AB mixing with the poor concentration coming from the GE (6), producing a high concentration (1), which is sent back to the GE via the SP, raising its pressure (2). After, the strong solution is preheated through SHX (3), using the heat of the weak solution stream coming from the GE (4) got a lower temperature in the poor concentration (5) and sent back to the AB through the SEV.

In the GE, the strong solution is heated until it boils applying external heat and refrigerant vapor is produced (7). Subsequently, it flows into the CO until saturated liquid (8). Furthermore, the refrigerant liquid goes directly to the REV, reducing its pressure and temperature, becoming a two-phase mixture (9). Then, the refrigerant enters the E where it is boiled by the heat absorbed from the refrigerated space until it becomes saturated vapor (10) and then, the cycle is repeated. The difference between the *HR-ARS* cycle concerning the conventional *ARS* system is that both, the refrigerant produced in the

generator (7) as well as the weak solution (4) give up heat to the strong solution (3) in the SHX causes that the generator thermal load decrease and the performance of the HR-ARS can be improved.

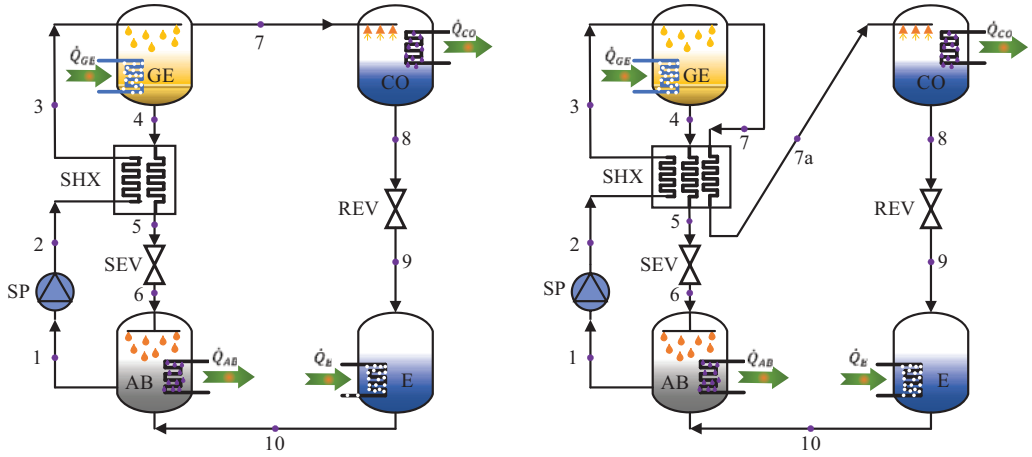

(a) Conventional *ARS* (b) Alternative *HR-ARS*

Figure 1: Schematic of conventional *ARS* and alternative *HR-ARS*

2.2 First Law Analysis and Assumptions

For the simulation of the *HR-ARS* and the conventional *ARS* cycle, mass and energy conservation analysis are applied in each component of the system. The simulation was made under steady-state conditions and the effects of potential and kinetic energies are negligible. The main equations of each component of both cycles are described as follows:

Mass balance

$$\sum \dot{m}_i = \sum \dot{m}_e \tag{1}$$

Mass concentration balance

$$\sum \dot{m}_i x_i = \sum \dot{m}_e x_e \tag{2}$$

Energy balance

$$\sum \dot{Q} - \sum \dot{W} = \sum \dot{m}_e h_e - \sum \dot{m}_i h_i \tag{3}$$

For the simulation of the systems, is necessary to adopt the following assumptions:

1. Steady-state conditions.
2. The potential and kinetic energy effects are insignificant.
3. The pressure drop through the components is considered to be negligible, except in the expansion valves.
4. The heat losses in the system components are negligible.
5. The poor concentration and the refrigerant at the outlet of the generator and evaporator are as saturated vapor, while strong concentration and the refrigerant leaving the absorber and condenser are as saturated liquid.

6. The refrigerant vapor entering the condenser is considered as superheated vapor.
7. Refrigerant and strong solution have the same temperature at the outlet and inlet of the solution heat exchanger.
8. The temperature and pressure of the dead state are considered as 25°C and 1.013 bar, respectively.

The energy balance in each of the components of the *ARS* and *HR-ARS* systems is given by the equations presented in Table 1.

Table 1: Energy equations for the conventional *HR-ARS* and *ARS* systems

Component	Energy balance
Evaporator	$\dot{Q}_E = \dot{m}_{10}\,(h_{10} - h_9)$
Absorber	$\dot{Q}_{AB} = \dot{m}_{10}h_{10} + \dot{m}_6h_6 - \dot{m}_1h_1$
Condenser (*ARS*)	$\dot{Q}_{CO} = \dot{m}_7\,(h_7 - h_8)$
Condenser (*HR-ARS*)	$\dot{Q}_{CO} = \dot{m}_{7a}\,(h_{7a} - h_8)$
Generator	$\dot{Q}_{GE} = \dot{m}_7h_7 + \dot{m}_4h_4 - \dot{m}_3h_3$
Solution throttling valve	$h_5 = h_6$
Solution pump	$\dot{W}_{SP} = \dot{m}_1\,(h_2 - h_1)$
Refrigerant throttling valve	$h_8 = h_9$
Solution heat exchanger (*ARS*)	$\dot{Q}_{SHX} = \dot{m}_4\,(h_4 - h_5)$
	$\dot{Q}_{SHX} = \dot{m}_2\,(h_3 - h_2)$
Solution heat exchanger (*HR-ARS*)	$\dot{Q}_{SHX} = \dot{m}_2\,(h_3 - h_2)$
	$\dot{m}_2h_2 + \dot{m}_7h_7 + \dot{m}_4h_4 = \dot{m}_3h_3 + \dot{m}_5h_5 + \dot{m}_{7a}h_{7a}$

A parameter used to measure the energy efficiency in an absorption chiller is called the coefficient of performance (*COP*), which is defined as the ratio of cooling production ($\dot{Q}_E$) concerning the total energy supplied ($\dot{Q}_{GE} + \dot{W}_{SP}$). In the *HR-ARS* and *ARS* systems, the coefficient of performance can be calculated using the following equation [24,25]:

$$COP = \frac{\dot{Q}_E}{\dot{Q}_{GE} + \dot{W}_{SP}} \tag{4}$$

To improve the *COP* of *HR-ARS* and *ARS* systems, a solution heat exchanger is used between the generator and absorber. Then, the efficiency of the solution heat exchanger is evaluated by the following expression [26,27]:

$$\eta_{SHX} = \frac{T_4 - T_5}{T_4 - T_2} \tag{5}$$

3 Second Law Analysis

The second law of thermodynamics consists of evaluating the exergy performance in a system, whose reduction is associated with losses in the components system. According to Asensio-Delgado et al. [28], exergy can be defined as the maximum useful power that can be produced by a system or flow. Besides, Jiménez-García et al. [29] used Eq. (6) to calculate the irreversibility in an

absorption chiller:

$$I = \sum \dot{E}_i - \sum \dot{E}_e + \left[\sum \left(\dot{Q}\left(1 - \frac{T_0}{T}\right)\right)_i - \sum \left(\dot{Q}\left(1 - \frac{T_0}{T}\right)\right)_e\right] \pm \sum \dot{W} \tag{6}$$

where, I is the internal irreversibility of the system, $\dot{Q}\left(1 - \frac{T_0}{T}\right)$ and $\dot{W}$ are the exergy loss associated with heat transfer rate and the mechanical power transferred to or from the control volume, respectively, while $\dot{E}$ is the exergy loss of each stream, which is calculated by the following equation:

$$\dot{E} = \dot{m}\left[(h - h_0) - T_0\,(s - s_0)\right] \tag{7}$$

Applying Eq. (6) in the *HR-ARS* and *ARS* systems, the irreversibility for each component is shown in Table 2. Furthermore, the total irreversibility in the system is calculated by the following expression:

$$I_{Total} = I_E + I_{AB} + I_{CO} + I_{GE} + I_{SP} + I_{REV} + I_{SEV} + I_{SHX} \tag{8}$$

Table 2: Irreversibility in each component for the *HR-ARS* and *ARS* systems

Component	Exergy balance
Evaporator	$I_E = \dot{m}_9\,(e_9 - e_{10}) + \dot{Q}_{EV}\left(1 - \frac{T_0}{T_r}\right)$
Absorber	$I_{AB} = \dot{m}_{10}e_{10} + \dot{m}_6 e_6 - \dot{m}_1 e_1 - \dot{Q}_{AB}\left(1 - \frac{T_0}{T_{AB}}\right)$
Condenser	$I_{CO} = \dot{m}_7\,(e_7 - e_8) - \dot{Q}_{CO}\left(1 - \frac{T_0}{T_{CO}}\right)$
Condenser (*HR-ARS*)	$I_{CO} = \dot{m}_{7a}\,(e_{7a} - e_8) - \dot{Q}_{CO}\left(1 - \frac{T_0}{T_{CO}}\right)$
Generator	$I_{GE} = \dot{m}_3 e_3 - \dot{m}_4 e_4 - \dot{m}_7 e_7 + \dot{Q}_{GE}\left(1 - \frac{T_0}{T_{GE}}\right)$
Solution pump	$I_{SP} = \dot{m}_1\,(e_1 - e_2) + \dot{W}_{SP}$
Refrigerant throttling valve	$I_{REV} = \dot{m}_8\,(e_8 - e_9)$
Solution throttling valve	$I_{SEV} = \dot{m}_5\,(e_5 - e_6)$
Solution heat exchanger (*ARS*)	$I_{SHX} = \dot{m}_4\,(e_4 - e_5) + \dot{m}_2\,(e_2 - e_3)$
Solution heat exchanger (*HR-ARS*)	$I_{SHX} = \dot{m}_4\,(e_4 - e_5) + \dot{m}_2\,(e_2 - e_3) + \dot{m}_7\,(e_7 - e_{7a})$

The exergy efficiency is the reason the exergy produced respect the exergy input, which can be obtained by the following expression [30]:

$$\eta_{ex} = \frac{\dot{Q}_E\left(1 - \frac{T_0}{T_r}\right)}{\dot{Q}_{GE}\left(1 - \frac{T_0}{T_{GE}}\right) + \dot{W}_{SP}} \tag{9}$$

The exergetic performance also can be defined as the ratio of the exergy rate produced and the exergy of the fuel [31,32], which can be calculated according to the following equation:

$$\eta_{ex} = \frac{\dot{E}_P}{\dot{E}_F} = 1 - \frac{I_{Total}}{E_F} \tag{10}$$

4 Model Verification

To verify the current model, energy and exergy results for the *ARS* cycle have been compared with those results obtained by Arora et al. [33] under the same operating conditions ($T_{GE} = 87.8°C$, $T_{CO} = T_{AB} = 37.8°C$, $T_E = 7.2°C$, $\eta_{IHX} = 70\%$ and refrigerant mass flow rate = 1 kg/s). Table 3 shows that the maximum relative deviation between both models was 1.40%, then, according to the comparison, the accuracy of the model was verified.

Table 3: Comparison of the proposed model with theoretical results of Arora et al. [33]

Component	Unit	Arora et al. [33]	Present work	Deviation (%)
Generator	kW	3095.698	3093.106	0.083
Condenser	kW	2505.910	2505.910	0.000
Evaporator	kW	2355.450	2355.450	0.000
Absorber	kW	2945.269	2942.678	0.087
SHX	kW	518.717	522.588	0.746
Solution pump	kW	0.03143	0.03099	1.400
COP	(–)	0.7609	0.7615	0.078
Exergetic efficiency	%	11.75	11.76	0.085
Total irreversibilities	kW	475.36	474.90	0.096

5 Model Validation

The validation of the present simulation was compared with experimental data presented by Florides et al. [34], considering the following operating conditions: $T_{GE} = 90°C$, $T_{CO} = 44.3°C$, $T_{AB} = 34.9°C$, $T_E = 6°C$, solution heat exchanger effectiveness ($\eta_{SHX} = 0.522$) and cooling capacity of 10 kW and the results are showed in Table 4. It can be seen that the deviations are less than 1.4% ratifying the exactitude of our model.

Table 4: Validation of the present simulation with experimental data from Florides et al. [34]

Component	Unit	Florides et al. [34]	Present work	Deviation (%)
Generator	kW	14.20	14.23	0.21
Condenser	kW	10.78	10.63	1.39
Evaporator	kW	10.00	10.00	0.00
Absorber	kW	13.51	13.60	0.66
COP	(–)	0.704	0.702	0.078

Simulation and Operating Conditions

The simulation has been developed using the computational software EES [35] to carry out the energy and exergy analysis of *HR-ARS* and *ARS* cycles. The choice of this software is justified because it contains the thermodynamic and transport properties of LiBr-H_2O. To investigate the energetic and exergetic efficiencies of the alternative *HR-ARS* cycle and compare it with the basic *ARS* system, the input operating conditions shown in Table 5 were used.

Table 5: Working parameters used in the *HR-ARS* and *ARS* systems

Parameter	Values	Unit
Generator temperature, T_{GE}	60 to100	°C
Evaporator temperature, T_E	5 to15	°C
Condenser temperature, T_{CO}	25 to 40	°C
Absorber temperature, T_A	25 to 40	°C
Refrigerated object temperature, T_r	$T_E + 5$	°C
Refrigerant mass flow rate, $\dot{m}_r$	1	kg/s

6 Results and Discussion

The influence of the main working conditions on the energy and exergy performance in the alternative *HR-ARS* and conventional *ARS* is studied. Moreover, the comparison between the exergy destruction in the alternative *HR-ARS* and the conventional *ARS* is also examined.

6.1 Variation of T_{GE} and T_{CO} on COP

Fig. 2 displays the variations of *COP* with T_{GE} and $T_{CO} = T_A$ (30°C, 35°C and 40°C). For the analysis, T_E and η_{SHX} are kept fixed as 5°C and 0.7, respectively. From the results, it is observed an increase of the *COP* in the *ARS* and *HR-ARS* as the in the generator temperature increases. Initially it increases until an optimal value and then it decreases slowly, these behaviors are in concordance with the results obtained by Ahmad et al. [12]. It is due to that, to increase T_{GE} causes that the concentration circulation ratio decreases and subsequently, the energy supplied in the generator also decreases. The reason for this effect is showed in Fig. 2. It also can be found that the *HR-ARS* system presents a higher *COP* than the conventional *ARS* system over the entire range of generator temperatures. Furthermore, to reduce T_{CO} from 40°C to 30°C, reduces T_{GE} to approximately 22°C, while the *COP* for the *ARS* and *HR-ARS* can be improved by around 5.77% and 6.33%, respectively. Comparatively, the *COP* for the *HR-ARS* system is 2.57% higher than the *ARS* system at $T_{CO} = 40$°C. However, when the condenser temperature is reduced at $T_{CO} = 35$°C and 30°C, the *COPs* for the *HR-ARS* system results be 2.86% and 3.11% higher than the ones obtained by the *ARS* system. Also, it is obtained that the maximum $COP = 0.8173$ in the *HR-ARS* is found at $T_{CO} = 30$°C, but at $T_{CO} = 35$°C and 40°C these values are of 0.785 and 0.756, respectively. In contrast, in the *ARS* system, the maximum *COPs* at the considered condenser temperatures are 0.801, 0.766 and 0.737, respectively. The former is because, if T_{CO} decreases, P_{GE} also decreases, so that the heat supplied in the generator is reduced and then, the *COP* of the systems will be improved.

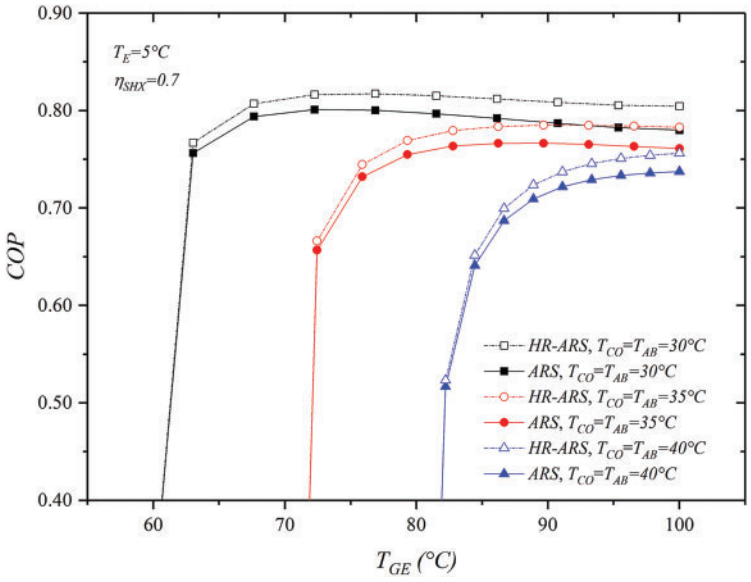

Figure 2: Variations of *COP* with T_{GE} for the *HR-ARS* and conventional *ARS* at different condenser temperatures

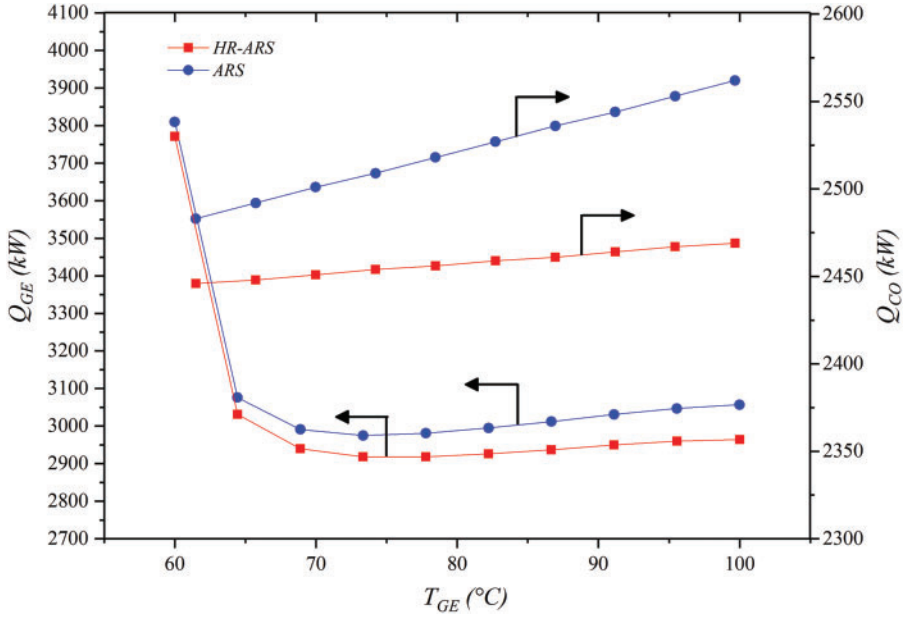

Figure 3: Effect of T_{GE} on Q_{GE} and Q_{CO} for the *HR-ARS* and *ARS*

6.2 Variation of T_{GE} on Q_{GE} and Q_{CO}

Fig. 3 shows the influence of T_{GE} on the Q_{GE} *and* Q_{CO} in the alternative *HR-ARS* and *ARS* systems. It can be seen that the load in the generator is reduced between 26% to 28% in both systems as T_{GE} increases and for high T_{GE}, the thermal load in the generator becomes almost constant, while the condensation heat increases between 1.2% to 3.3% as the generation temperature also is

increased. Lamine et al. [36] have found that the generator load is reduced with increasing the generator temperature, although condenser heat increases slightly. Reductions of 21% in the generator's heat load have also been found by Marashli et al. [37] in a basic LiBr/Water absorption chiller varying the generator temperature from 95°C to 105°C. For all ranges of generator temperatures, the thermal load in the generator and condenser results be lower in the *HR-ARS* system than in the conventional *ARS*. It is due to that in the *HR-ARS* system, part of the heat in the condenser is recovered via the solution heat exchanger, then the temperature and enthalpy at the inlet in the generator (Point 3) increase and the temperature at the inlet in the condenser (Point 7a) is reduced, so lower energy in the generator and condenser is required. Under the operating conditions of $T_E = 5$°C, $T_{CO} = T_{AB} = 30$°C and $\eta_{SHX} = 0.7$, the heat supplied in the *HR-ARS* system is around 1.51%–3.76% lower than the one required in the *ARS* system. On the other hand, at $T_{GE} = 60$°C, the condensation heat for the *HR-ARS* system is 1.51% less than the conventional *ARS*, but when the generation temperature is increased at $T_{GE} = 100$°C, it can be reduced up to 3.76%. It leads to a reduction in the heat exchanger area and the manufacturing cost of the condenser and generator are minor than the basic *ARS*.

Fig. 4 illustrates the variations of the *COP* for the *HR-ARS* and *ARS* cycles with respect to the condenser temperature (T_8). For the study, both the condenser and absorber were considered to be at the same temperature ($T_{CO} = T_{AB}$). The *COP* was analyzed under three different generator temperatures ($T_{GE} = 80$°C, 90°C and 100°C) and kept as constant $T_E = 5$°C and solution heat exchanger effectiveness = 0.7 in order to cover a greater range of operating conditions. It was found that raising T_{CO} reduces the coefficient of performance in both systems and these behaviors have also been found by Kaynakli et al. [38]. When $T_{GE} = 80$°C, the reductions are around 23%, but at generator temperatures of $T_{GE} = 90$°C and 100°C, the reductions are around 11% and 9%, respectively. The reason is because, when the condenser and absorber temperature increase, the generation pressure also becomes higher and the strong solution concentration at the generator inlet is reduced, then, the thermal load of the generator rises and the *COP* of the systems gets worse.

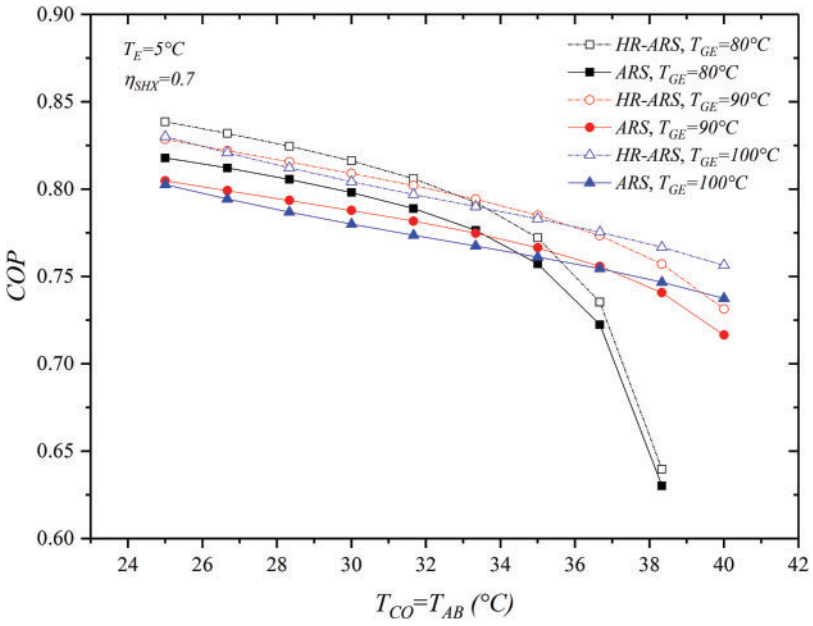

Figure 4: Influence of $T_{CO} = T_{AB}$ on *COP* for the *HR-ARS* and conventional *ARS*

The highest energy performance is obtained at low condenser and generator temperatures. For example, at $T_{CO} = 25°C$ and $T_{GE} = 80°C$, the COP for the *HR-ARS* and *ARS* systems is 0.8386 and 0.8179, respectively. When T_{GE} rises at $T_{GE} = 90°C$, the highest COPs for the *HR-ARS* and *ARS* are 0.8286 and 0.8048, but at $T_{GE} = 100°C$, energy performances are 0.8026 and 0.8301, respectively. In comparison, the COP for *HR-ARS* is between 2.53%–3.42% higher than that for *ARS*. The results also show that at generator temperatures of 100°C and 90°C, both systems can work without problem in all range of condenser temperatures, although, at $T_{GE} = 80°C$, these only can operate in a condenser and absorber temperature range of 25°C–38.3°C.

Finally, the highest energy performances are found at $T_{GE} = 80°C$ and $T_{CO} < 33°C$, while for a $T_{GE} = 100°C$, is recommended to work both systems at $T_{CO} > 36.66°C$ to reach the highest energy performances.

The influence of T_E on *COP* in the alternative and conventional *ARS* systems is shown in Fig. 5. In these calculations, $T_{CO} = T_{AB} = 30°C$, $T_{GE} = 80°C$, 90°C and 100°C, $\eta_{SHX} = 0.7$ were assumed. As it is expected, increasing T_E has a positive effect on the *COP* and this is slightly higher as T_{GE} decreases [39]. This is clarified by the fact that less refrigerant capacity is produced from the evaporator as T_E decreases, then if T_E is increased better *COP* is obtained and it is higher than one with a lower T_E. On the other hand, at higher generator temperatures, more refrigerant mass rate is produced, improving the *COP* in both systems.

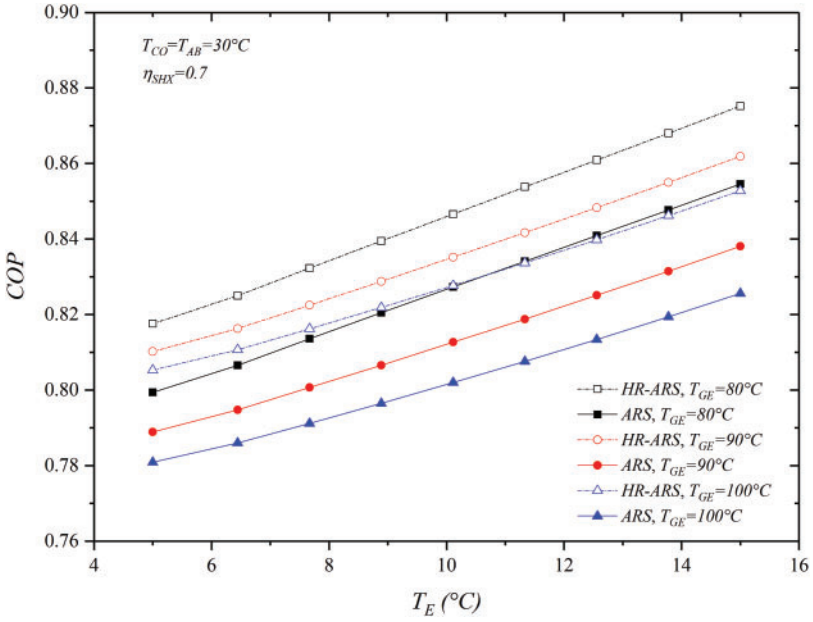

Figure 5: Effect of T_E on COP for the *HR-ARS* and *ARS*

The best coefficient of performance is obtained at the lowest generator temperature ($T_{GE} = 80°C$) and the highest evaporator temperatures ($T_E = 15°C$), while the lowest one corresponds at high generator temperatures ($T_{GE} = 100°C$). For a $T_{GE} = 80°C$ and T_E ranging from 5°C to 15°C, the *COP* in the *HR-ARS* increases by 8.06% and for the *ARS*, the increase is 7.89%. When the generator temperature is raised at $T_{GE} = 90°C$, the *COP* increases by 7.20% and 7.03%, respectively. However, at $T_{GE} = 100°C$, the *COP* augmentation is 6.40% and 6.60%, respectively. It was found that the *COP* for

the *HR-ARS* cycle is around 3% superior to that found with the ARS at the three different generator temperatures here analyzed.

Fig. 6 depicts the effect of η_{SHX} on the *COP* at different generator temperatures (T_{GE} = 80°C, 90°C and 100°C) for the proposed *HR-ARS* system as well as for the conventional *ARS*, considering as constant the evaporation and condensing temperatures of 5°C and 30°C, respectively. It can be seen that the *COP* for both cycles increases as η_{SHX} effectiveness increases and these trends are like for the generator temperatures here studied, which is in concordance with those results obtained by References [27,38]. The reason for this change is that as the η_{SHX} effectiveness increases, the generator temperature entering the generator also increases, reducing the thermal load in the generator, which results be lower for the *HR-ARS* system than that required for the *ARS* system.

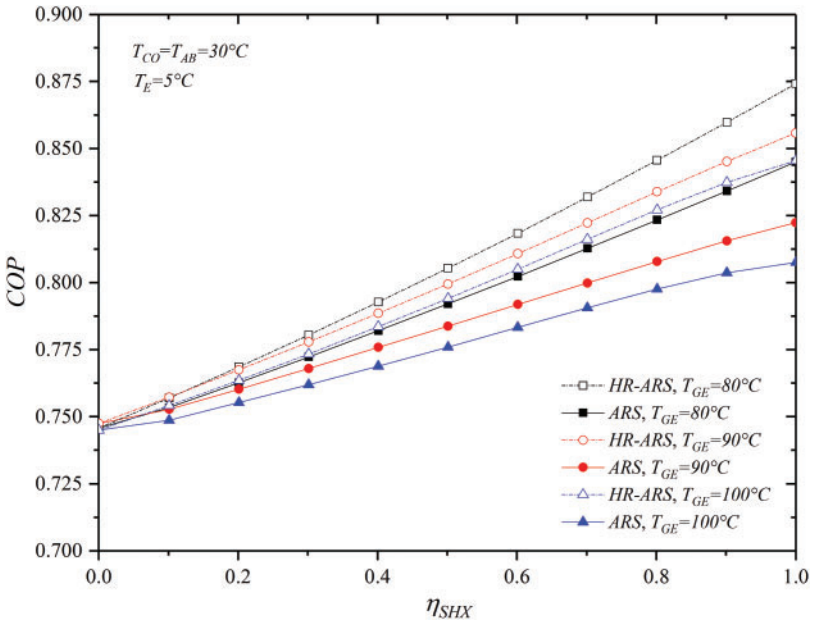

Figure 6: Effect of η_{SHX} on the *COP* for different T_{GE} values

The results also show that for all η_{SHX} effectiveness and T_{GE} range, an increase between 8.40%–19.25% on the *COP* is found for the *ARS* cycle. When the *HR-ARS* cycle is used, these increases vary between 13.48%–22.62%, which means that the *HR-ARS* is better in 3.37% to 5.08% than the conventional *ARS* system. It also is appreciated that the *COP* is lower as T_{GE} rises. It is because, if the generator temperature gets higher, the concentration difference between the weak and strong solution also increases, then improves the *COP* for both systems. For example, at a η_{SHX} = 1 and T_{GE} = 80°C, the *COP* for the *HR-ARS* cycle is 0.874 and at T_{GE} = 100°C is 0.845, while for the *ARS* system, the *COPs* obtained are 0.845 and 0.807, respectively. In comparison, the *HR-ARS* has between 3.43%–4.70% higher *COP* than the conventional *ARS* system at the mentioned generator temperatures.

Fig. 7 illustrates the influence of T_{GE} on the exergetic performance of the *HR-ARS* and *ARS* systems at different condenser temperatures and fixed values of evaporation temperature and solution heat exchanger effectiveness at 5°C and 0.7, respectively. The results show that the exergy efficiency is higher as the generator temperature rises, as well as the condenser temperature decreases, then, it reaches an optimum value and after is reduced. These observations also have been found by Kaushik et al. [40] in a conventional absorption cycle for T_{GE} varying from 55°C–105°C and T_{CO}

values of 30°C, 35°C and 40°C. The before is because a high generator temperature produces more vapor refrigerant, however, it implies a higher heat input to the system and then, the irreversibilities in the generator also increase. However, reducing the condenser temperature increases the refrigerant effect and reduces the irreversibility in the cycle, improving the energy and exergy performance.

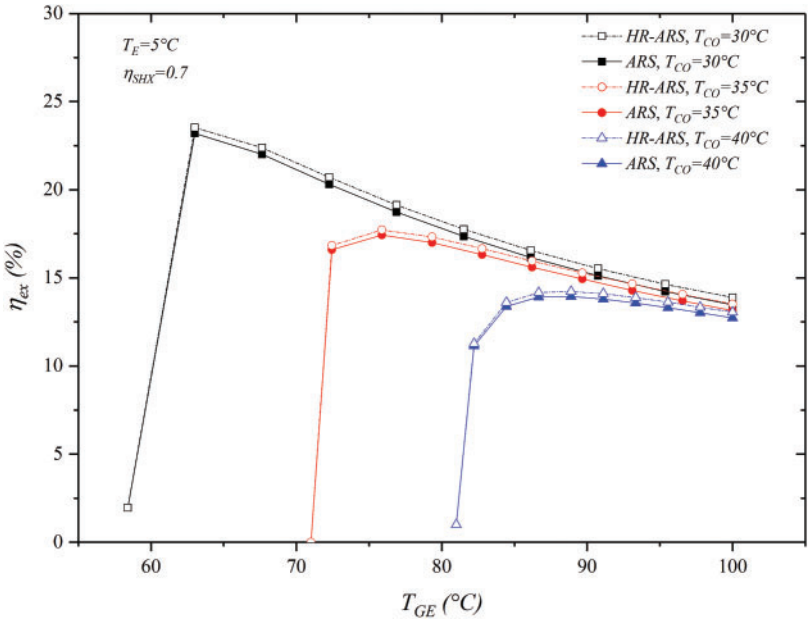

Figure 7: Effect of T_{GE} on η_{ex} for the *HR-ARS* and conventional *ARS* at different condenser temperatures

From the figure, it is found that at $T_{CO} = 30$°C, the maximum exergy efficiency of 23.53% and 23.22% are obtained with the *HR-ARS* and *ARS* systems at the corresponding generator temperature of 63.02°C. When the condenser temperature rises to 35°C, the optimum exergy efficiency obtained for both systems are 17.72% and 17.43%, respectively, which are found at a generator temperature of 67.64°C. However, at $T_{CO} = 40$°C, its maximum exergy efficiency is 14.23% and 13.95%, respectively, at $T_{GE} = 76.88$°C. The results also show that at $T_{GE} = 100$°C, the exergetic efficiencies for the considerate condenser temperatures are very similar.

The influence of T_E and T_{GE} on exergy performance for *HR-ARS* and *ARS* was studied and compared, taking as constant $T_{CO} = T_{AB} = 30$°C and a solution heat exchanger effectiveness = 0.7, and its behavior is shown in Fig. 8. When T_E increases, the exergy efficiency is reduced between 17%–20%, and this increases between 2.3%–6.3% as the generator temperature decreases. As is presented in the figure, the highest exergetic efficiency for the *HR-ARS* ($\eta_{ex} = 29.49\%$) and *ARS* ($\eta_{ex} = 28.84\%$) are obtained at low evaporator and generator temperatures ($T_E = 5$°C and $T_{GE} = 80$°C), while that at the same T_E and $T_{GE} = 100$°C, the lowest exergetic efficiency for the *HR-ARS* and *ARS* are $\eta_{ex} = 22.57\%$ and $\eta_{ex} = 21.89\%$, respectively. It means that at the mentioned evaporator and generator temperatures, the exergetic performance for the *HR-ARS* is around 0.7% superior that the traditional *ARS*. It also is found that, when the evaporator temperature is increased until $T_E = 15$°C, the exergetic efficiency for the *HR-ARS* system is very similar for the three generator temperatures under study, showing only a difference of 0.22% with respect to the values found for the conventional *ARS* system.

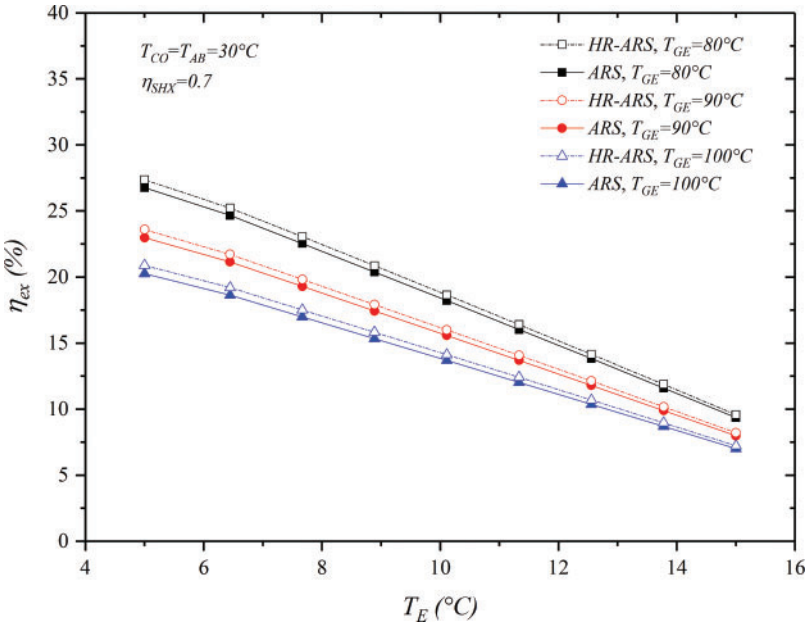

Figure 8: Effect of T_E on η_{ex} for the *HR-ARS* and conventional *ARS* at different generator temperatures

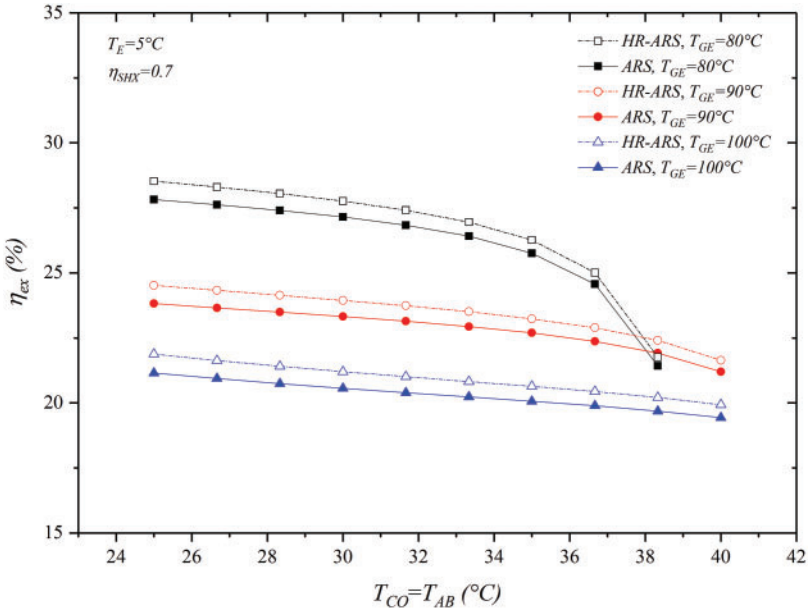

Figure 9: Influence of $T_{CO} = T_{AB}$ on η_{ex} for the *HR-ARS* and conventional *ARS*

Fig. 9 shows the influence of $T_{CO} = T_{AB}$ on the exergetic efficiency of both systems. A reduction in the exergy efficiency is found as $T_{CO} = T_{AB}$ increases, and this is more significant as the generator temperature decreases at 80°C. It was found that when T_{GE} = 90°C and 100°C are considered, the systems can operate in the entire temperature range in the condenser, while at the generator temperature of 80°C, both systems work adequately at condenser temperatures between 25°C to

38.33°C. Furthermore, when the systems work with the lowest T_{GE} and T_{CO}, the highest exergetic efficiencies can be obtained, while the lowest ones are found at high generator temperatures.

The results also show that the highest exergetic efficiency of 28.53% is obtained with the *HR-ARS* system operates at $T_{CO} = 25°C$ and $T_{GE} = 80$°C, but it is reduced by 4.02% and 6.63% when the T_{GE} decreases from 90°C and 100°C, respectively. At condensation and generator temperatures of 40°C and 100°C, respectively, the exergy efficiency is 19.93% for the *HR-ARS* system and 19.43% for the *ARS*. However, by reducing the generator temperature to 90°C, the exergy efficiency increases by 8.58% with the *HR-ARS* and 9.10% with the *ARS* system. It also found that the *HR-ARS* presents between 2.55% to 3.33% higher exergy performance when T_{CO} varies from 25°C to 40°C, in comparison with those results found with the *ARS* system.

The variations of the exergetic efficiency with η_{SHX} and T_{GE} in both systems are shown in Fig. 10. The exergetic efficiency increases as η_{SHX} increases and decreases as T_{GE} is reduced. The best exergy efficiency values are obtained in both systems at the maximum solution heat exchanger effectiveness. Furthermore, when η_{SHX} varies from 0 to 1, the exergy efficiency for the *HR-ARS* system increases between 14.88% to 20.07%, while for the conventional *ARS* refrigeration system, the increases are in the order of 9.79% to 16.05%. The results also show that at the maximum charge of the solution heat exchanger, the exergy efficiency of the *HR-ARS* cycle is between 3.43%–4.70% higher than the *ARS* system. When both systems work without a solution heat exchanger, the exergy efficiency at $T_{GE} =$ 80°C is 16.04%, while when T_{GE} is increased to 90°C and 100°C, the exergy efficiencies are 14.10% and 12.56%, respectively. This represents that at the generator temperature of 80°C, the exergy efficiency is 1.94% and 3.48% higher than that at generator temperatures of 90°C and 100°C, respectively.

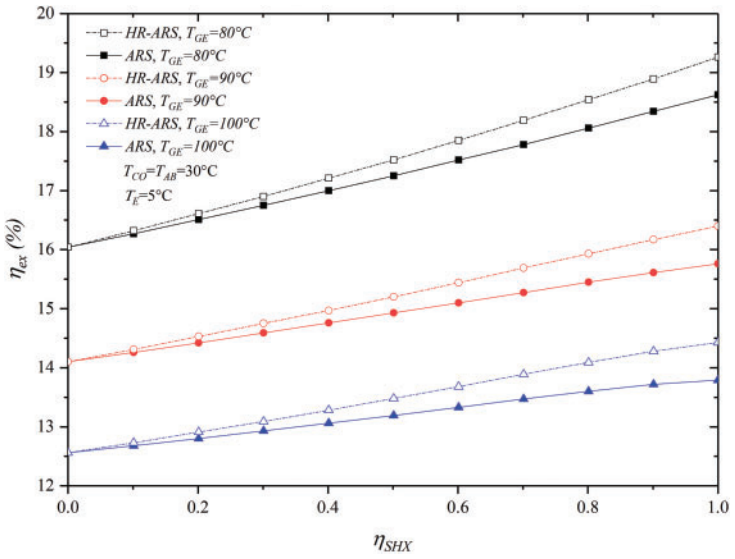

Figure 10: Effect of η_{SHX} on η_{ex} for the *HR-ARS* and conventional *ARS*

Fig. 11 illustrates the impact of T_{GE} on the exergy destruction in the different components of the *HR-ARS* and *ARS* cycles. As the generator temperature increases, the absorber, generator and condenser increase their exergy destruction rate, while the opposite situation occurs with the evaporator, refrigerant throttling valve and solution heat exchanger. It was found that the evaporator, generator and absorber are the main components to contribute to the total exergy destroyed. At low generator temperatures, the evaporator has the highest exergy destruction with around 49%, followed

by the absorber with 17% and the generator with 12%, while at high generator temperatures (T_{GE} = 100°C), the largest contributors to the irreversibilities of the system are the absorber (38%), generator (36%) and evaporator (20%). The condenser and refrigeration expansion valve do not contribute significantly to the total exergy destruction.

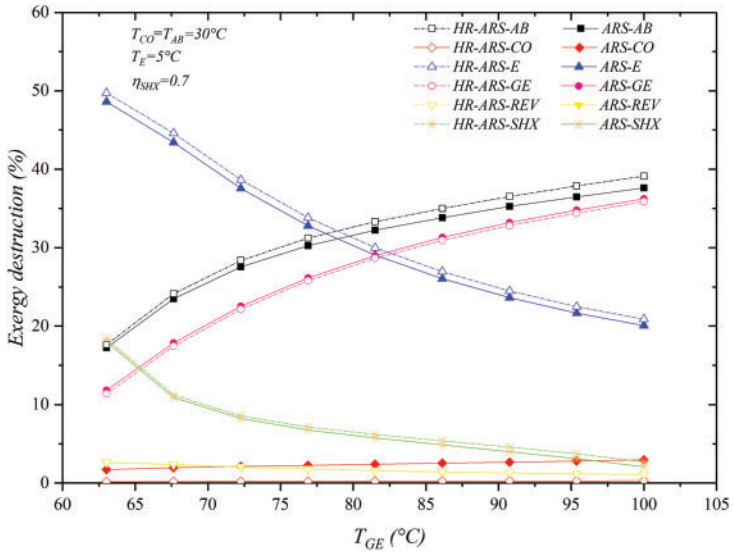

Figure 11: Effect of T_{GE} on *exergy destruction* for the *HR-ARS* and conventional *ARS*

The irreversibilities in the evaporator are due to the difference of temperature between the surroundings and the fluid, but the irreversibilities in the absorber are caused by the difference of temperature between the component and the environment, which can be reduced by increasing its surface area, while the exergy destruction in the generator is outstanding to the difference of temperatures between the heat source and the working mixture. It can be also seen that, for all range of generator temperatures, the exergy destroyed in the absorber and generator increase in 21.49% and 24.51%, respectively, while in the evaporator and solution heat exchanger it is reduced 28.87% and 15.95%, respectively. From the figure, it is seen that the irreversibilities for the *HR-ARS* system are slightly superior to the *ARS* system in the most of the components, except for the condenser and generator, which are reduced in 0.47% and 2.65%, respectively.

Finally, in order to improve the second law efficiency, more emphasis could be made in the evaporator, absorber and generator in the overall design.

Fig. 12 shows the behavior of the destroyed exergy concerning the condensation temperature. The results show a reduction in the exergy destroyed in the absorber and generator as T_{CO} increases, while the opposite situation occurs with the evaporator, solution heat exchanger and refrigerant throttling valve as the temperature condensation increases, except in the condenser, where no significant variations are shown. It can be observed that the exergy destroyed in the absorber and generator are very similar at low condenser temperatures (T_{CO} = 25°C) and these components are responsible to contribute in almost 80% of the overall exergy destroyed, similar percentages have also been found by Cai et al. [41]. It can also be observed that the exergy destroyed in the solution heat exchanger resulted higher for the other components at T_{CO} > 37°C, while the exergy destruction is slightly reduced in the evaporator, refrigerant valve and condenser.

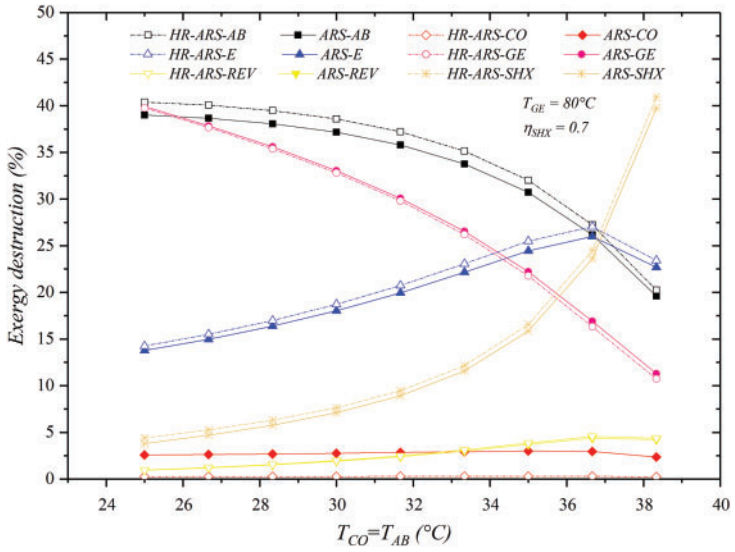

Figure 12: Effect of $T_{CO} = T_{AB}$ on *exergy destroyed* for the *HR-ARS* and *ARS*

For the entire temperature range in the condenser, the exergy destroyed for the absorber and generator is reduced by 19.4% and 28.64%, while for the case of the evaporator, solution heat exchanger and refrigerant valve, the exergy destruction increases by 8.9%, 35.95% and 3.30%, respectively. For high condenser temperatures ($T_{CO} = 40$°C), the largest exergy destroyed is obtained in the solution heat exchanger, followed by the evaporator, absorber and generator. It was found that in both systems, the largest exergy destroyed corresponds to the solution heat exchanger at $T_{CO} > 36.66$°C.

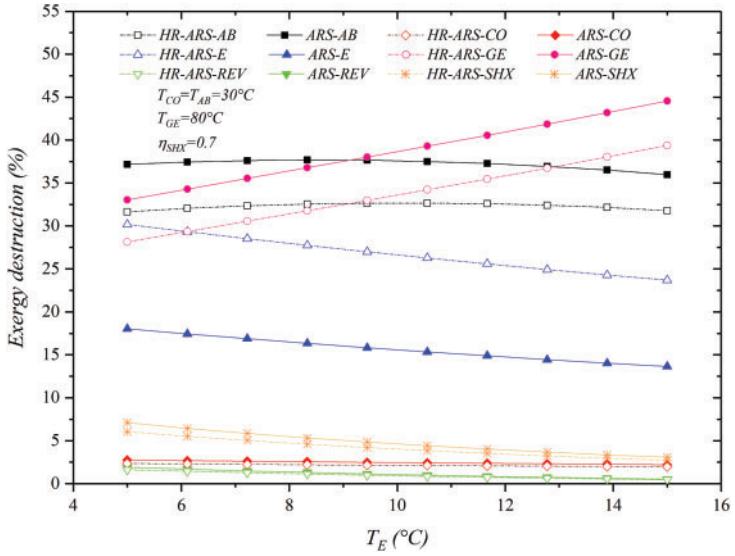

Figure 13: Effect of T_E on exergy destruction for the *HR-ARS* and conventional *ARS*

Fig. 13 shows the influence of the evaporation temperature on the exergy destroyed for the *HR-ARS* and *ARS* systems. If T_E is increased, the exergy destroyed in the generator also increases, although the opposite occurs with the other components in both systems. The results also show that the

evaporation temperature does not present significant effects on the exergy destroyed in the throttling valve and condenser.

The results reveal that of the overall exergy destroyed, 88% is mainly outstanding to the absorber, generator and evaporator in both systems, which is obtained at $T_E = 5°C$. For a $T_E = 15°C$, these components contribute to 94% of the total exergy destroyed. The absorber presents the largest amount of exergy destroyed at low evaporation temperatures, followed by the generator and absorber, while at high evaporation temperatures, the generator is the main component contributor to the exergy destruction. For evaporator temperatures ranging from 5°C to 15°C, the exergy destroyed in the generator increases by 12%, while for the absorber, evaporator, solution exchanger, condenser and refrigeration expansion valve, the exergy destroyed is reduced by approximately 1.19%, 4.39%, 4.04%, 0.54% and 1.38%, respectively. Comparatively, the exergy destroyed is lower for almost all of the components for the *HR-ARS* in all ranges of evaporator temperatures than the ones for the *ARS* system, except for the evaporator, which increases.

The contribution of the exergy destroyed for different solution heat exchanger effectiveness in each component for both systems is shown in Fig. 14. As depicted, the main contributor to the exergy destruction in the *HR-ARS* and *ARS* systems is the absorber. The other two components with significant exergy losses are the generator and condenser. It is also observed that as the η_{SHX} increases, the exergy destruction in the generator, SHX and condenser is reduced, while in the other components, there are no significant variations in the exergy destruction. When $\eta_{SHX} = 0.7$, the overall exergy destroyed for the *HR-ARS* is 3.24% smaller than the one found for the ARS system. Moreover, at $\eta_{SHX} = 0.8, 0.9$ and 1, the reductions in the total exergy destruction for the *HR-ARS* are 3.79%, 4.39% and 5.01%, all of these in comparison with the *ARS* system. This is due to an increase in the η_{SHX}, which increases the strong concentration temperature at the inlet of the generator reduces the inlet temperature in the condenser and the exergy in the Streams 3 and 11 as well as the heat supplied in the generator and condenser, reducing with this the irreversibilities in these components. Furthermore, the exergy loss in the solution heat exchanger is reduced because the difference in temperature between the poor and strong concentrations also is reduced.

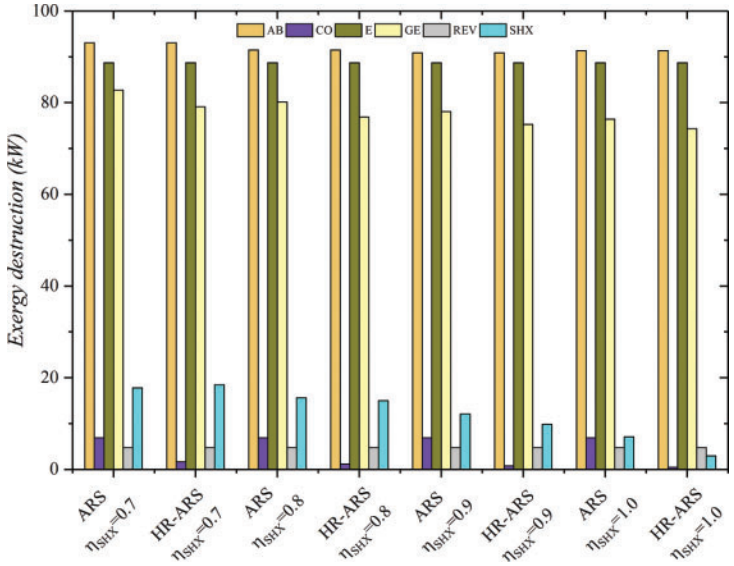

Figure 14: Contribution of *exergy destruction* for *HR-ARS* and *ARS* at different η_{SHX}

7 Conclusions

In this work, an alternative *ARS* configuration in which part of the thermal load in the condenser is recovered via the solution heat exchanger and supplied to the system *(HR-ARS)* was energy and exergy investigated. The influence of the main working parameter as well as the efficiency of the solution heat exchanger on the coefficient of performance, exergy performance and exergy destroyed for the *HR-ARS* system were analyzed and compared with the traditional *ARS* system at the same working conditions. The main conclusions of the simulation are described as follows:

1. The *COP* increases as T_{GE} and T_E increase, but it reduces as T_{CO} increases. The highest $COP = 0.8173$ is found with the *HR-ARS* at $T_{GE} = 80$°C and $T_{CO} = 30$°C. Comparatively, the *COP* for the *HR-ARS* is 2.57% higher than the *ARS* system at $T_{GE} = 80$°C and $T_{CO} = 40$°C. However, it can be improved by 2.86% when $T_{CO} = 35$°C and 3.11% when $T_{CO} = 30$°C.
2. For all ranges of generator temperatures, the thermal load in the generator and condenser in the *HR-ARS* are between 1.51%–3.76% and 1.2%–3.3% lower than the ones required in the *ARS* system. It leads to a reduction in the heat exchangers area, so the manufacturing cost of the alternative *HR-ARS* can be smaller than the *ARS* system.
3. The *COP* and exergy efficiency increase as η_{SHX} increases. The highest energy and exergy efficiency are obtained at $\eta_{SHX} = 1$. For η_{SHX} varying from 0 to 1, the exergy performance for the *HR-ARS* increases between 14.88% to 20.07%, while for the conventional *ARS* refrigeration system these increases are in the order of 9.79% to 16.05%. Which means that the *HR-ARS* system has 3.43%–4.70% higher exergy efficiency than the *ARS* system. On the other hand, for all ranges of solution heat exchanger effectiveness, the *HR-ARS* system showed 3.79%–5.01% lower exergy destroyed than *ARS*.
4. The exergy performance increases as the generator temperature rises, as well as when the condenser and evaporator temperature decrease. The largest values of exergy are obtained at the lowest generator, condenser and evaporator temperatures. The maximum exergy efficiency of 23.53% and 23.22% are found when the *HR-ARS* and *ARS* systems operate at $T_{CO} = 63.02$°C and $T_{CO} = 30$°C, but it is slightly lower as T_{CO} increases from 30°C to 40°C. It implies that the exergy performance with *HR*-ARS system is around 0.3% higher than the *ARS*. Furthermore, when T_E increases from 5°C to 15°C, the exergy efficiency is reduced between 17%–20%, and this increases between 2.3%–6.3% as the generator temperature decreases. For all ranges of evaporating temperatures, the exergy efficiency for the *HR-ARS* is between 0.22% to 0.7% higher than the traditional *ARS*.
5. The values of exergy destruction in the generator, absorber and evaporator increase as the generator temperature increases, while that opposite situation occurs with the other components of the system. On the other hand, when T_E rises, the exergy destroyed in the generator also rises. The results also showed a reduction in the exergy destroyed in the absorber and generator, while the exergy destruction in the evaporator, solution heat exchanger and refrigerant throttling valve rises if T_{CO} increases, except in the condenser, where no significant variations are shown. Furthermore, the exergy destruction for the *HR-ARS* resulted 3.24% lower than the *ARS* system at $\eta_{SHX} = 0.7$. However, when $\eta_{SHX} = 0.8$, 0.9 and 1 are used, *HR-ARS* showed 3.79%, 4.39% and 5.01% lower irreversibilities than the *ARS*.
6. Finally, the results revealed that the *HR-ARS* system can be a suitable alternative in the field of absorption refrigeration because lower energy is required, it has higher energy and exergy performance as well as lower exergy destruction than the *ARS* system.

Acknowledgement: The authors thank the Autonomous University of Hidalgo State for the support provided for the realization of this research paper.

Funding Statement: The authors not received funding for the realization of this study.

Author Contributions: The authors confirm contribution to the paper as follows: study conception and design: J. L. Rodríguez-Muñoz, J. S. Pacheco-Cedeño, I. J. González-Hernández; data collection: J. F. Ituna-Yudonago, J. J. Ramírez-Minguela; analysis and interpretation of results: J. L. Rodríguez-Muñoz, I. J. González-Hernández, J. S. Pacheco-Cedeño; draft manuscript preparation: J. L. Rodríguez-Muñoz, J. F. Ituna-Yudonago, J. J. Ramírez-Minguela. All authors reviewed the results and approved the final version of the manuscript.

Availability of Data and Materials: Data will be made available on request.

Ethics Approval: Not applicable.

Conflicts of Interest: The authors declare no conflicts of interest to report regarding the present study.

References

1. Al-Sayyab AKS, Mota-Babiloni A, Navarro-Esbrí J. Renewable and waste heat applications for heating, cooling, and power generation based on advanced configurations. Energy Convers Manag. 2023;291:117253. doi:10.1016/j.enconman.2023.117253.
2. Gürel AE, Yıldız G, Ergün A, Ceylan I. Exergetic, economic and environmental analysis of temperature controlled solar air heater system. Clean Eng Technol. 2021;6(2):100369. doi:10.1016/j.clet.2021.100369.
3. Belman-Flores JM, Barroso-Maldonado JM, Rodríguez-Muñoz AP, Camacho-Vázquez G. Enhancements in domestic refrigeration, approaching a sustainable refrigerator–a review. Renew Sustain Energ Rev. 2015;51(6):955–68. doi:10.1016/j.rser.2015.07.003.
4. Meraj M, Azhar M, Khan MZ, Salik Anjum MS, Sahil Faiz Ahmad M, Ab Rasheed MF, et al. Thermal modelling of PVT-CPC integrated vapour absorption refrigeration system. Mater Today: Proc. 2021;38(1–2):391–6. doi:10.1016/j.matpr.2020.07.547.
5. Braccio S, Phan HT, Wirtz M, Tauyeron N, Pierres N. Simulation of an ammonia-water absorption cycle using exchanger effectiveness. Appl Therm Eng. 2022;213:118712. doi:10.1016/j.applthermaleng.2022.118712.
6. Kumar A, Rakshit D. A critical review on waste heat recovery utilization with special focus on Organic Rankine Cycle applications. Clean Eng Technol. 2021;5(6):100292. doi:10.1016/j.clet.2021.100292.
7. Misenheimer CT, Terry SD. The development of a dynamic single effect, lithium bromide absorption chiller model with enhanced generator fidelity. Energy Convers Manage. 2017;150(193):574–87. doi:10.1016/j.enconman.2017.08.005.
8. Kallitsis K, Koulocheris V, Pappa G, Voutsas E. Evaluation of water + imidazolium ionic liquids as working pairs in absorption refrigeration cycles. Appl Therm Eng. 2023;233(1):121201. doi:10.1016/j.applthermaleng.2023.121201.
9. Aman J, Henshaw P, Ting DS-K. Bubble-pump driven LiBr-H_2O and LiCl-H_2O absorption air-conditioning systems. Thermal Sci Eng Progress. 2018;6(1998):316–22. doi:10.1016/j.tsep.2017.10.022.
10. Kumbhar A, Gulhane N, Pandure S. Theoretical analysis of hybrid chiller. Energy Proc. 2017;109:487–96. doi:10.1016/j.egypro.2017.03.082.

11. Ayou DS, Wardhana MFV, Coronas A. Performance analysis of a reversible water/LiBr absorption heat pump connected to district heating network in warm and cold climates. Energy. 2023;268:126679. doi:10.1016/j.energy.2023.126679.
12. Ahmad T, Azhar M, Sinha MK, Meraj M, Mahbubul IM, Ahmad A. Energy analysis of lithium bromide-water and lithium chloride-water based single effect vapour absorption refrigeration system: a comparison study. Cleaner Eng Technol. 2022;7:100432. doi:10.1016/j.clet.2022.100432.
13. Jeong J, Jung HS, Lee JW, Kang YT. Hybrid cooling and heating absorption heat pump cycle with thermal energy storage. Energy. 2023;283(1):129027. doi:10.1016/j.energy.2023.129027.
14. Wang J, Liu Z, Wang H, Lui H. A new combined cooling and power system based on ammonia-water absorption refrigeration cycle: thermodynamic comparison and analysis. Energy Convers Manag. 2022;270(13):116262. doi:10.1016/j.enconman.2022.116262.
15. Razmi A, Soltani M, Kashkooli FM, Garousi Farshi L. Energy and exergy analysis of an environment friendly hybrid absorption/recompression refrigeration system. Energy Convers Manag. 2018;164:59–69. doi:10.1016/j.enconman.2018.02.084.
16. Babaei SM, Razmi AR, Soltani M, Nathwani J. Quantifying the effect of nanoparticles addition to a hybrid absorption/recompression refrigeration cycle. J. Cleaner Prod. 2020;260(48):121084. doi:10.1016/j.jclepro.2020.121084.
17. Peng Z, Li Z, Zeng J, Yu J, Lv S. Thermo-economic analysis of absorption compression hybrid cooling systems with parallel subcooling and recooling for small scale low-grade heat source and low temperature application. Int J Refrig. 2022;138:220–32. doi:10.1016/j.ijrefrig.2022.03.003.
18. Wang J, Wang B, Wu W, Li X, Shi W. Performance analysis of an absorption-compression hybrid refrigeration system recovering condensation heat for generation. Appl Therm Eng. 2016;108:54–65. doi:10.1016/j.applthermaleng.2016.07.100.
19. Pacheco-Cedeño JS, Rodríguez-Muñoz JL, Ramírez-Minguela JJ, Pérez-García V. Comparison of an absorption-compression hybrid refrigeration system and the conventional absorption refrigeration system: exergy analysis. Int J Refrig. 2023;155(2):81–92. doi:10.1016/j.ijrefrig.2023.08.003.
20. Ochoa GV, Forero JD, Quinones LO. Exergetic analysis of a LiBr-H_2O singe effect absorption refrigeration system. Int J ChemTech Res. 2018;11:363–8. doi:10.20902/IJCTR.2018.110743.
21. Blanco-Marigorta AM, Marcos JD. Key issues on the exergetic analysis of H_2O/LiBr absorption cooling systems. Case Stud Therm Eng. 2021;28:101568. doi:10.1016/j.csite.2021.101568.
22. Banu PA, Premkumar TM, Sivamani S, Vijayabalan PA. Detailed second law (exergetic) analysis approach of H_2O-LiBr vapour absorption cooling system. IOP Conf Ser: Mater Sci Eng. 2020;998:01062. doi:10.1088/1757-899X/998/1/012062.
23. Mohtaram S, Chen W, Lin J. A study of an absorption refrigeration cycle by exergy analysis approach. IOP Conf Ser: Earth Environ Sci. 2018;182:012021. doi:10.1088/1755-1315/182/1/012021.
24. FathiAlmas Y, Ghadamian H, Aminy M, Moghdasi M, Amirian H, Hoeinadesh S, et al. Thermo-economic analysis, energy modeling and reconstructing of components of a single solar-absorption lithium bromide chiller for energy performance enhancement. Energy Build. 2023;285:112894. doi:10.1016/j.enbuild.2023.112894.
25. Abid M, Khan MS, Ratlamwala TA, Amber KP. Thermo-environmental investigation of solar parabolic dish-assisted multi-generation plant using different working fluids. Int J Energy Res. 2020;44(15):1–19. doi:10.1002/er.5340.
26. Herold K. Absorption chillers and heat pumps. Boca Raton: CRC Press; 2016.
27. Li Na, Luo C, Su QA. Working pair of $CaCl_2$-LiBr-$LiNO_3$/H_2O and its application in a single-stage solar driven absorption refrigeration cycle. Int J Refrig. 2018;86(2):1–13. doi:10.1016/j.ijrefrig.2017.11.004.
28. Asensio-Delgado JM, Asensio-Delgado S, Zarca G, Urtiaga A. Analysis of hybrid compression absorption refrigeration using low-GWP HFC or HFO/ionic liquid working pairs. Int J Refrig. 2022;134:232–41. doi:10.1016/j.ijrefrig.2021.11.013.

29. Jiménez-García JC, Rivera W. Exergy analysis of an experimental ammonia/water absorption cooling system. Case Stud Therm Eng. 2023;49:103167. doi:10.1016/j.csite.2023.103167.
30. Tenkeng M, Wouagfack PAN, Techinda R. Exergy analysis of a double-effect solar absorption refrigeration system in Ngaoundere. World J Eng Technol. 2019;7(1):158–74. doi:10.4236/wjet.2019.71011.
31. Mohtaram S, Omidi M, Lin J, Sun H, Chen W. Exergy analysis of a multi mixture working fluid absorption refrigeration cycle. Case Stud Therm Eng. 2019;15(4):100540. doi:10.1016/j.csite.2019.100540.
32. Zhang Ke, Ma H, Li Q, Wang D, Song Q, Wang X, et al. Thermodynamic analysis and optimization of variable effect absorption refrigeration system using multi-island genetic algorithm. Energy Rep. 2022;8:5443–54. doi:10.1016/j.egyr.2022.04.004.
33. Arora A, Kaushik SC. Theoretical analysis of $LiBr/H_2O$ absorption refrigeration systems. Int Energy Res. 2009;33(15):1321–40. doi:10.1002/er.1542.
34. Florides GA, Kalogirou SA, Tassou SA, Wrobel LC. Design and construction of a LiBr-water absorption machine. Energy Convers Manag. 2003;44(15):2483–508. doi:10.1016/S0196-8904(03)00006-2.
35. Klein SA. Engineering equation solver (EES), version 10.2. Madison, USA: F-Chart Software; 2020. Available from: www.fchart.com/. [Accessed 2024].
36. Lamine CM, Said Z. Energy analysis of single effect absorption chiller ($LiBr/H_2O$) in an industrial manufacturing of detergent. Energy Proc. 2014;50:105–12. doi:10.1016/j.egypro.2014.06.013.
37. Marashli A, Alfanatseh E, Shalby M, Gomaa M. Modelling single-effect of Lithium Bromide-Water driven by an evacuated solar tube collector in Ma'an city (Jordan) case study. Case Stud Therm Eng. 2022;37(2):102239. doi:10.1016/j.csite.2022.102239.
38. Kaynakli O, Kilic M. Theoretical study on the effect of operating conditions on performance of absorption refrigeration system. Energy Convers Manag. 2007;48(2):599–607. doi:10.1016/j.enconman.2006.06.005.
39. Ghatos S, Janan MT, Mehdari A. Thermodynamic model of a single stage H_2O-LiBr absorption cooling. E3S Web Conf. 2021;234:00091. doi:10.1051/e3sconf/202123400091.
40. Kaushik SC, Arora A. Energy and exergy analysis of single effect and series flow double effect water-lithium bromide absorption refrigeration systems. Int J Refrig. 2009;32(6):1247–58. doi:10.1016/j.ijrefrig.2009.01.017.
41. Cai D, He G, Tian Q, Tang W. Exergy analysis of a novel air-cooled non-adiabatic absorption refrigeration cycle with NH_3–NaSCN and NH_3–$LiNO_3$ refrigerant solutions. Energy Convers Manag. 2014;88:66–78. doi:10.1016/j.enconman.2014.08.025.